Geophys. J. Int. (2004) **159,** 9–16 doi: 10.1111/j.1365-246X.2004.02385.x

Application of SAR interferometry to a large thrust deformation: the 1999 $M_w = 7.6$ Chichi earthquake in central Taiwan

C. P. Chang,[1] C. T. Wang,[1] T. Y. Chang,[2] K. S. Chen,[1] L. S. Liang,[1] E. Pathier[3] and J. Angelier[3]

[1] *Center for Space and Remote Sensing Research, National Central University, Chungli* 320, *Taiwan. E-mail: cpchang@csrsr.ncu.edu.tw*
[2] *Institute of Geophysics, National Central University, Chungli, Taiwan*
[3] *Laboratoire de Tectonique Quantitative, Université P. & M. Curie, Paris, France*

Accepted 2004 June 16. Received 2004 June 15; in original form 2002 September 16

SUMMARY

Application of the interferometric method to four ERS2-SAR images acquired before and after the 1999 Chichi earthquake has allowed determination of the coseismic surface displacement in the footwall area of the Chelungpu fault. The interferometric results revealed a relative shortening in the round trip distance between the radar antenna and the ground of the footwall side of Chelungpu fault, during the earthquake. This shortening progressively increased from the west to the east and reaches the maximum amount of approximately 26 cm near the central segment of the Chelungpu fault. Our interferometric results have been precisely examined using a dense GPS network in the investigated area. We mapped the GPS coseismic measurements into the radar line of sight and implemented a forward simulation of SAR interferogram from this synthesized result to control our unwrapping performance. In this study, these two observations are compared with a 3-D dislocation model of the fault. Finally, a deformation analysis based on our interferometric result has indicated that a segment with irregular deformation behaviour can be distinguished in the footwall area of the Chelungpu fault. This segment may result from either the influence of inherited basement faults or the presence of a structural terrace that provide local opportunities for superficial deformation.

Key words: Chichi earthquake, SAR interferometry, Taiwan.

1 INTRODUCTION

The Chichi earthquake (M_w 7.6) that struck central Taiwan on 1999 September 20 (UTC) caused heavy casualties and widespread damage. As a result of the unprecedented amount of high-quality near-field data it generated (e.g. Teng *et al.* 2001), it is recognized as one of the most important earthquakes to date for the study of earthquake mechanics. In practice, this wealth of data not only allows more precise determination of faulting models for this event, but also addresses new questions concerning surface behaviour in the near field. Based on the dense geodetic and seismographic instrumentation in central Taiwan, which is spanned by a network of GPS stations, ground-motion accelerometers and broad-band seismometers, the characteristics of coseismic deformation related to the Chichi earthquake has been examined in detail (Ma *et al.* 1999; Shin *et al.* 2000; Yu *et al.* 2001). Integration of these measurements has shown that major coseismic displacement and crustal deformation occurred in the hangingwall of the Chelungpu fault, the main thrust fault reactivated in the Chichi earthquake (Fig. 1). On the western side of the fault, the footwall area showed relatively little deformation (e.g. Ma *et al.* 2000; Lee *et al.* 2001; Rubin *et al.* 2001; Yu *et al.* 2001) and the characteristics of surface movement in the footwall area were relatively poorly understood. Moreover, in view of the westward propagation of the deformation front in Taiwan (Suppe 1981), it may well be that the footwall area of the Chelungpu fault is incubating a future large thrust earthquake and warrants high attention in terms of risk mitigation.

Because it operates at microwave frequencies, the Synthetic Aperture Radar interferometry (InSAR) technique can determine surface displacement to centimetre scales. It is considered capable of detecting the spatial variation in the small displacement that occurred in the footwall area of the Chelungpu fault. The aim of this paper is to characterize the coseismic deformation of the footwall area in detail. First, we used GPS data to simulate the SAR interferogram. Secondly, we analysed four pairs of space-borne SAR images to extract the coseismic displacement using the interferometric method. The synthetic interferogram constructed using GPS data was compared to our interferometric results to control the possible orbit error and the unwrapping uncertainty in the interferometric analysis. We also compared our InSAR results with a 3-D elastic rebound model of fault dislocation to derive a more thorough understanding of the footwall deformation.

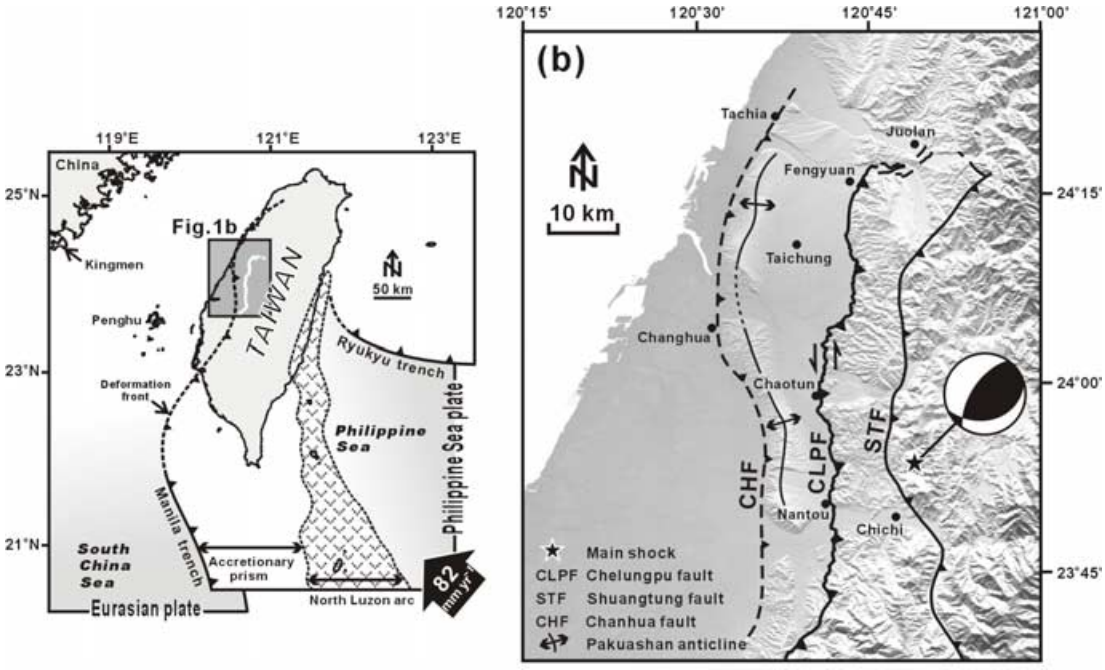

Figure 1. (a) Geodynamic framework of Taiwan. The large black arrow shows the convergence between the Philippine Sea Plate and the Eurasian continental margin (Yu *et al.* 1997). The area of Fig. 1(b) is indicated as a small rectangle in grey. The Chelungpu fault is highlighted by a thick white line. (b) The topography and major structures of the study area. The epicentre of the Chichi main shock is marked as a black star. Its focal mechanism, determined by the Central Weather Bureau, exhibits a thrust-dominant movement.

2 GEOLOGICAL SETTING

The recently uplifted mountain belt of Taiwan (since 5 Ma), with active faulting and deformation, affects a broad region (Suppe 1981; Chang & Chi 1983). The development of this mountain belt is interpreted as a consequence of convergence between the Philippine and Eurasian plates (for example, Ho 1986; Tsai 1986). Geodetic measurements during 1990–1995 (Yu *et al.* 1997) detecting a steady convergence rate greater than 8 cm yr^{-1} between the North Luzon arc and the Penghu islands, which belong to the Philippine Sea Plate and Eurasian Plate, respectively (Fig. 1a).

Because the Taiwan island is under an intense compressional tectonic regime, there have been more than 10 disastrous earthquakes reported in the past century. The most recent one, the Chichi earthquake, occurred in central Taiwan in 1999. Studies of the Chichi earthquake show that the main fault plane dips 29° eastwards down to approximately 15 km in depth (Kao & Chen 2000). During this earthquake, an approximately 80-km-long upthrust unit underwent displacement of several metres upwards and westwards along the Chelungpu thrust fault (Fig. 1b). A picture of the coseismic displacement of the Chelungpu fault derived from near-field GPS surveys (Yu *et al.* 2001) showed that the amount of slip gradually increased from approximately 2 m in the south to approximately 8 m in the north, in agreement with field studies along the fault trace (Hou *et al.* 2000; Chen *et al.* 2001; Lee *et al.* 2001).

The Chelungpu fault extends along the western front of the Taiwan mountain range (Fig. 1). In terms of stratigraphy, this front separates the rugged foothills of Miocene–Pliocene rocks to the east from the basins, tableland and coastal plain of Quaternary alluvial deposits to the west. Since approximately 1 Ma, the total contraction across the Chelungpu fault system (including adjacent thrusts) has reached approximately 10–15 km, measured from the latest geological balanced cross-sections (Mouthereau *et al.* 2001), although a greater degree of shortening has previously been inferred (suggested by Suppe 1981, 1983).

The topography on the footwall of the Chelungpu fault is relatively flat and the main land covers are urban areas or agricultural farm lands. Thus, this area is suitable for application of the InSAR technique. The topography of this area is caused by a regional curvature of the western deformation front of Taiwan (Fig. 1), where the Pakuashan anticline and the related Changhua thrust fault are located. The Pakuashan anticline is mainly composed of thick Pleistocene terrigenous sequences derived from the Central Range, which is overlain by uplifted, weathered and tilted late Quaternary fluvial material (Sun 1965; Liew 1988). The sigmoid shape of the present-day Taiwan deformation front in the Pakuashan–Changhua fold–thrust area is probably the result of Quaternary tectonic activity corresponding to the western propagation of convergent stresses within an arc–continent collision zone (Deffontaines *et al.* 1997).

3 FORWARD SIMULATION FROM GPS DATA

We projected the GPS coseismic measurements (data after Yu *et al.* 2001) into the range direction of the satellite and then converted the projected value into the phase domain to simulate the radar interferogram. The GPS data used in this study were collected from several campaigns mainly conducted by (i) the Central Geological Survey, Ministry of Economic Affairs, (ii) the Satellite Survey Division and Land Survey Bureau, Ministry of Interior and (ii) the Institute of Earth Sciences, Academia Sinica. The GPS measurements were collected within ∼ 2–32 months before and 3 months after the main shock of the Chichi earthquake. In Fig. 2, the horizontal displacement of the GPS stations with respect to the Kingmen station (Fig. 1a) represents a convergent setting with a fan-shaped distribution that increases from west to east. The maximum horizontal

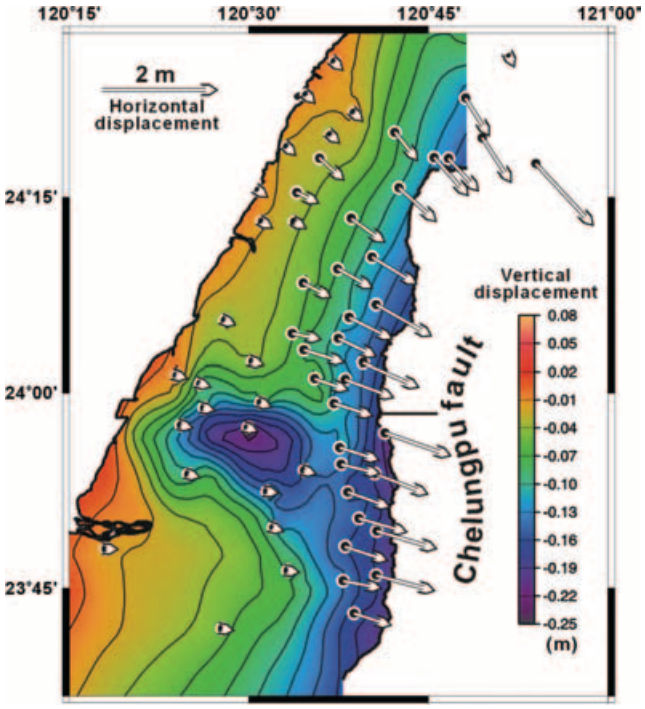

Figure 2. Coseismic displacement associated with the Chichi earthquake measured by the GPS stations in central Taiwan. Horizontal displacements relative to Kingmen (location see Fig. 1) are shown in vectors. The vertical displacement field was reconstructed from interpolated GPS data between stations (data after Yu *et al.* 2001).

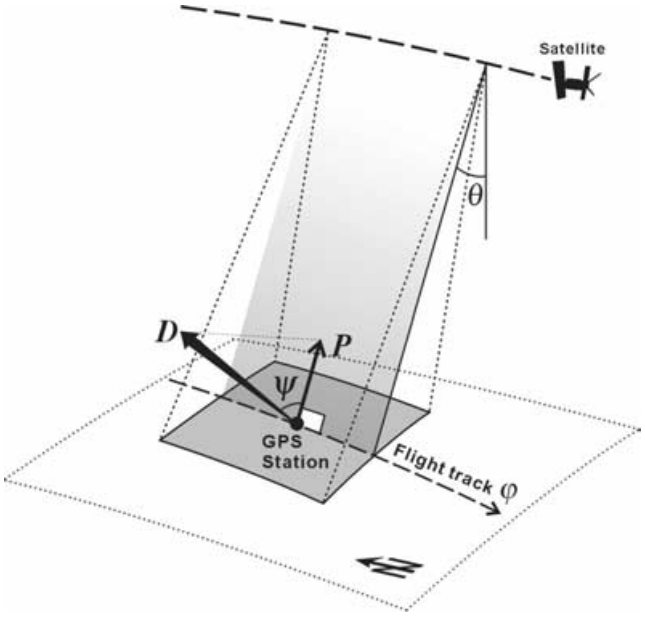

Figure 3. Schematic of projecting measured GPS displacement onto radar line of sight. **D** is the measured vector describing the motion of the GPS station. **P** is the projected vector of **D** onto the radar line of sight. ψ is the angle between the vectors **D** and **P**. φ and θ are the heading azimuth and look angle of the radar, respectively. The value of θ varies from near-range to far-range area, with the range 21° to 27° over an image scene.

displacement occurs immediately next to the Chelungpu fault. The direction of horizontal displacement is subperpendicular to the principal structures and the trend of the mountain range of the region. The vertical displacement field reveals subsidence with a progressive increase in magnitude from the west coast to the east (Fig. 2). In general, the GPS measurements indicate an eastward subsidence for the material lying on the footwall of the Chelungpu fault.

To simulate the interferogram of the C-band radar image, we first projected each GPS displacement vector (in three components) onto the slant range direction as shown in Fig. 3. This projection is equivalent to constructing the inner product of the measured vector from the GPS station and the direction of the radar line of sight, which increases from the near range to the far range (Fig. 3). After obtaining the projected displacement in the slant range direction from all GPS measurements, a composite map covering the entire study area was constructed by interpolating the available data points using a continuous curvature algorithm, which can prevent undesired oscillation and false local maxima and minima (Smith & Wessel 1990). Fig. 4(a) presents the synthetic slant range displacement derived from the scattered GPS measurements.

In the following, we create a synthetic interferogram from the value of composite map in Fig. 4(b). Except for some cyclic fringes in the central-western part and some boundary effects in the northern and southern ends, this synthetic interferogram generally shows a smooth, semi-elliptical pattern of fringes in the footwall area of the Chelungpu fault. This represents a possible InSAR feature and should be compared with the real interferometric results.

In Fig. 2, the GPS measurements revealed that the subsidence of the footwall block progressively increases from west to east. However, the synthesized interferogram shows a progressive shortening of the distance between the ground surface and the satellite from the western coast to the central segment of the Chelungpu fault (Figs 4a and b). As a result of the (projection) geometry, the radar interferogram shows only a component of the total displacement; Fig. 4(c) shows the geometric framework of the fault plane, the radar line of sight and the ground displacement in the footwall. At locations next to the rupture trace, the displacement in the footwall can be decomposed into horizontal movement towards the rupture plane ($\mathbf{D}_H$ in Fig. 4c) and vertical subsidence ($\mathbf{D}_V$). If the target moves toward the rupture plane with a depression angle (ω in Fig. 4c) smaller than the look angle of the satellite (θ), the distance between the satellite and the target would shorten although the target is experiencing subsidence relative to its previous state. In our case, the ground is moving toward the rupture plane with depression angle less than 10°, which smaller than the look angle of the satellite (approximately 23° at the scene centre); the simulated slant range displacement (**P**) near the Chelungpu fault reveals therefore a shortening pattern (Fig. 4c).

4 INSAR OBSERVATIONS

4.1 Method and data acquisition

Radar interferometry is a technique for extracting information on changes in the shape of the surface of the Earth by using the phase content of the radar signal (see, for example, Zebker *et al.* 1994; Massonnet & Feil 1998). We apply this technique, using SAR images acquired by the ERS2 satellite. The phase difference between two images acquired at different times creates an interference pattern called an interferogram (Massonnet & Feil 1998). The interferogram shows the change in range from ground to satellite, that is, the component of the displacement vector of the surface that points toward the satellite. The adjacent two fringes of the same colour (a phase variation of 2π radians) represent 28 mm of range change for ERS2. Such an interferogram records crustal deformation during the

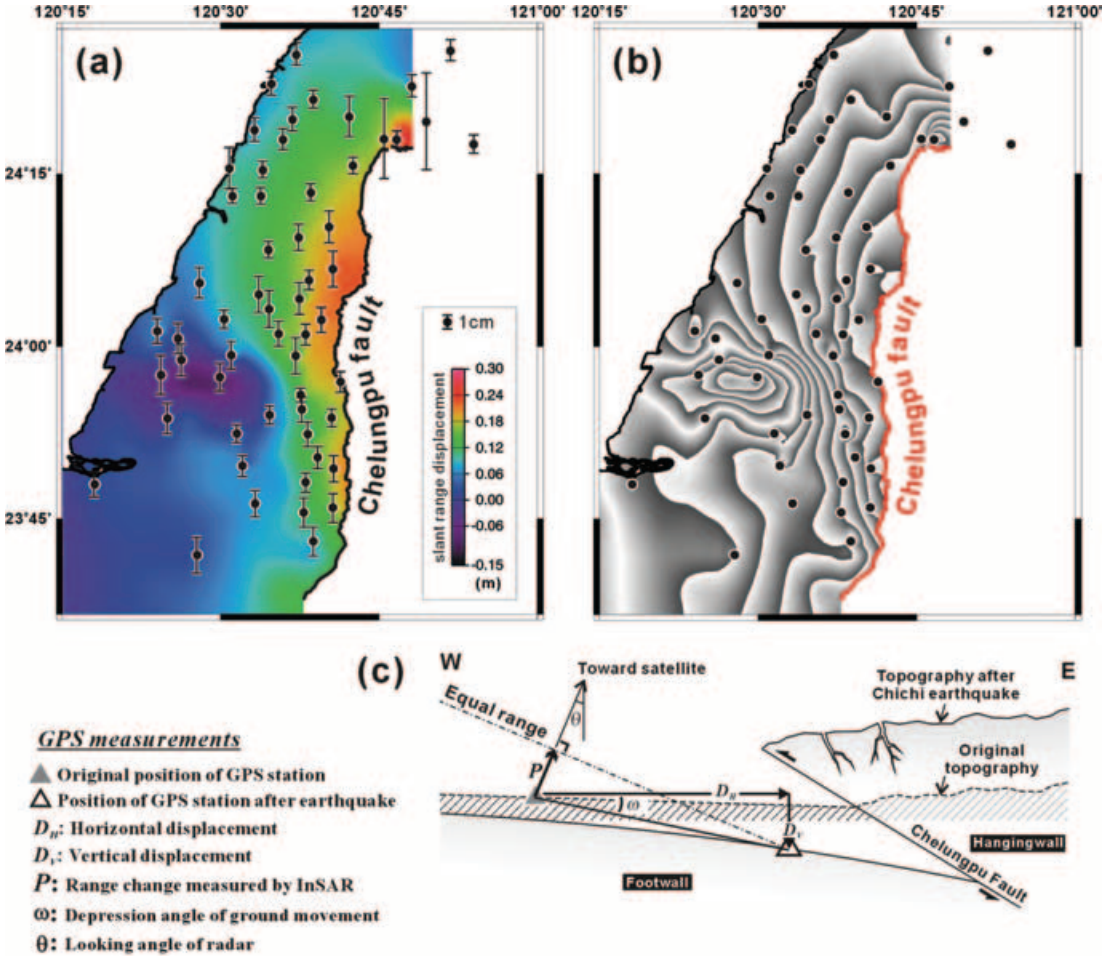

Figure 4. (a) Near-field coseismic slant range displacement estimated from GPS measurements. Error bars (95 per cent confidence) in slant range have been indicated for each station (data after Yu *et al.* 2001). (b) Synthetic interferogram from GPS measurements. Each fringe corresponds to 2.8 cm of slant range change. (c) Cross-section perpendicular to the flight track of the satellite showing the geometric relationship between the ground displacement and the slant range change. In general, land subsidence should cause slant range lengthening. However, in the case of the Chichi earthquake, the large amount of horizontal displacement from west to east produces a greater range shortening and counteracts the lengthening caused by the land subsidence.

time interval between the acquisitions of two images (for example, Burgmann *et al.* 2000).

The pairs of scenes that we used in our interferometric analysis are listed in Fig. 5. We selected two scenes (1999 January 21 and May 6) before the main shock and two scenes (1999 September 23 and October 28) after it, to extract the possible coseismic surface deformation. To obtain acceptable interferometric results, we need to use image pairs with small baselines (Wright *et al.* 1999). However, the images obtained immediately prior to the Chichi earthquake did not provide a good baseline condition. Therefore, it was necessary to consider a longer time interval before the earthquake. After the Chichi earthquake, the baseline condition is better, especially for the image acquired at 1999 October 28; collocated with the image acquired at 1999 May 6, this pair provides a very small perpendicular baseline (only 6 m) and a good altitude of ambiguity (of approximately 1570 m) at the scene centre (pair-3 in Fig. 5).

In this study, we use the two-pass approach implemented by the GAMMA software (http://www.gamma-rs.ch/) to obtain the interferogram. In the resulting interferograms, topographic fringes were removed using the Taiwanese digital elevation model (DEM, from the Taiwan Forestry Bureau) with a grid spacing of 40 m and average elevation accuracy of 1 m retrieved from 1:5000 topographic

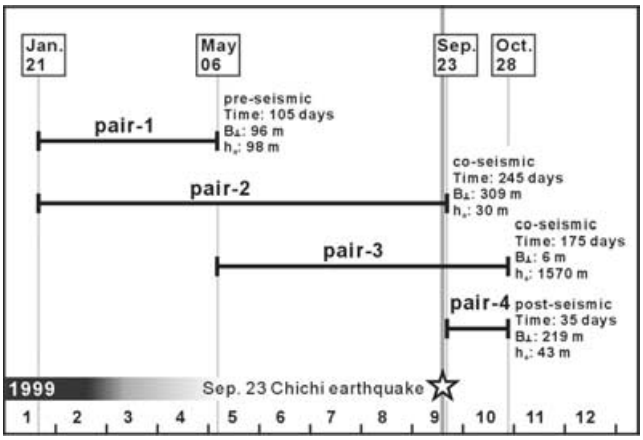

Figure 5. ERS2-SAR data pairs used in this study. The area studied is covered by one ERS2-SAR scene (descending orbit, track 232, frame 3123). Date of acquisition, interval time, vertical baseline offset ($B_\perp$) and altitude of ambiguity (h_a) are shown.

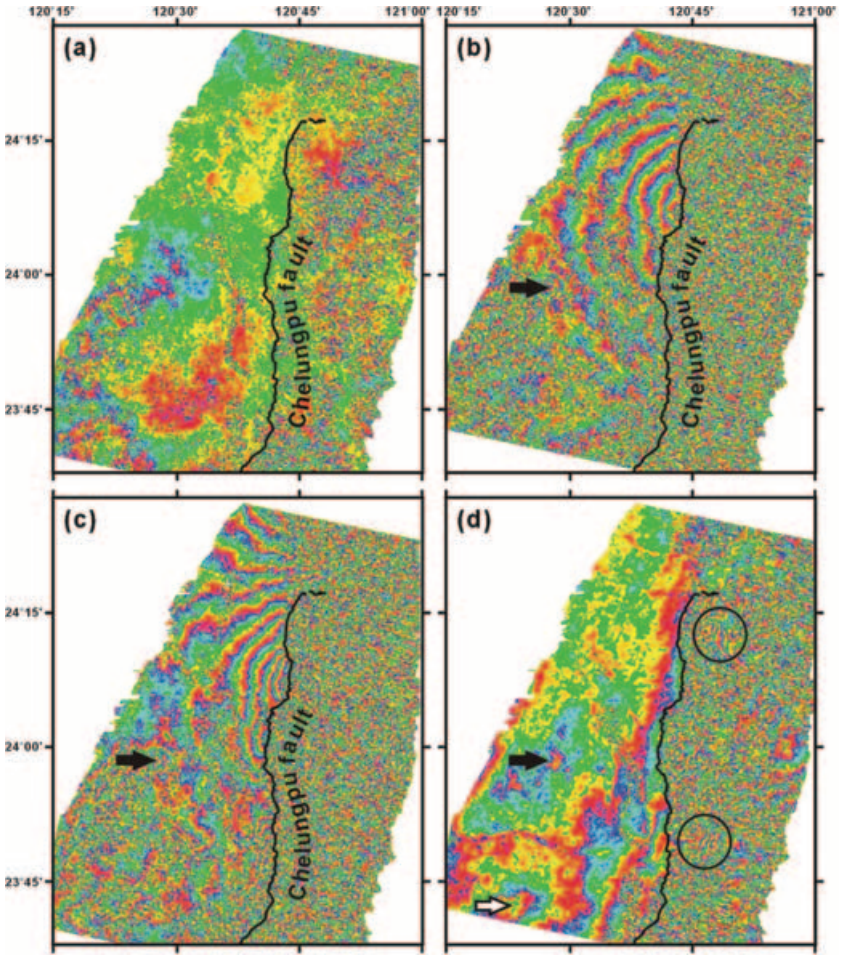

Figure 6. Differential interferograms correspond with the ERS2/SAR data pairs in Fig. 5. (a) Pair-1, (b) pair-2, (c) pair-3, and (d) pair-4.

maps. The topographic relief at the footwall area of the Chelungpu fault is generally small (the altitude of the highest hill is approximately 400 m). With the good altitude of ambiguity, the effect of topography is very small and the error was well controlled. Because the details of this technique have been described elsewhere (for example, Massonnet & Feil 1998; Burgmann *et al.* 2000), we restrict our discussion to interpreting the interferogram in terms of crustal deformation.

4.2 Interferometric results

Four pairs of SAR data were processed from single-look complex (SLC) images to generate the differential interferograms (Fig. 6). In spite of our careful image selection, the radar correlation in the hangingwall area of the Chelungpu fault still breaks down, whereas on the relatively flat footwall area, where human activity abounds, the image coherence is good even for image pairs that include the earthquake event.

In the pair-1 interferogram, acquired before the main shock of the Chichi earthquake (Fig. 5), the absence of clear interferometric fringes suggests that there was no detectable deformation before the earthquake (Fig. 6a). In contrast, for image pair-2 and pair-3, selected to contain the time of the Chichi main shock (Fig. 5), concentric fringe patterns are clearly present in the footwall area (Figs 6b and c). The fringes in both interferograms could be considered as indicators of the possible coseismic displacement of this area. In terms of the round trip distance change between the radar antenna and the ground, both these interferometric fringe patterns represent a relative shortening that increases from the west coast toward the central segment of the Chelungpu fault.

The interferogram simulated from GPS data could be applied to control the possible orbit error in the interferometric result (for example, Hudnut *et al.* 1994; Burgmann *et al.* 2002; Delouis *et al.* 2002; Donnellan *et al.* 2002; Feigl *et al.* 2002). After a rough comparison, we find that our simulated interferogram (Fig. 4b) has a very similar fringe pattern to the real InSAR results (Figs 6b and c). This suggests that the orbit error in these two interferograms is negligible and that additional fine-tuning for these fringe patterns may be unnecessary. In practice, the range change profiles shown in Fig. 7(b) further support this view; the general slope of the simulated interferogram (from GPS data) matches that of the interferometric result in this study very well (see also the Discussion, Section 5).

The poor interferometric result in respect of the hangingwall of the Chelungpu fault deserves some attention. There may be two principal causes, which may have acted together. The first cause could come from the dense vegetation. East of the Chelungpu fault, the hills and mountains are covered by dense forest and fruit trees, so it is more difficult to detect possible displacement using the C-band SAR. The second cause is that the amount of displacement in the hangingwall area is too large in this earthquake event (approximately 5 m in general after previous field studies). Because the C-band SAR allows measurement of movements only in the centimetre scale, the

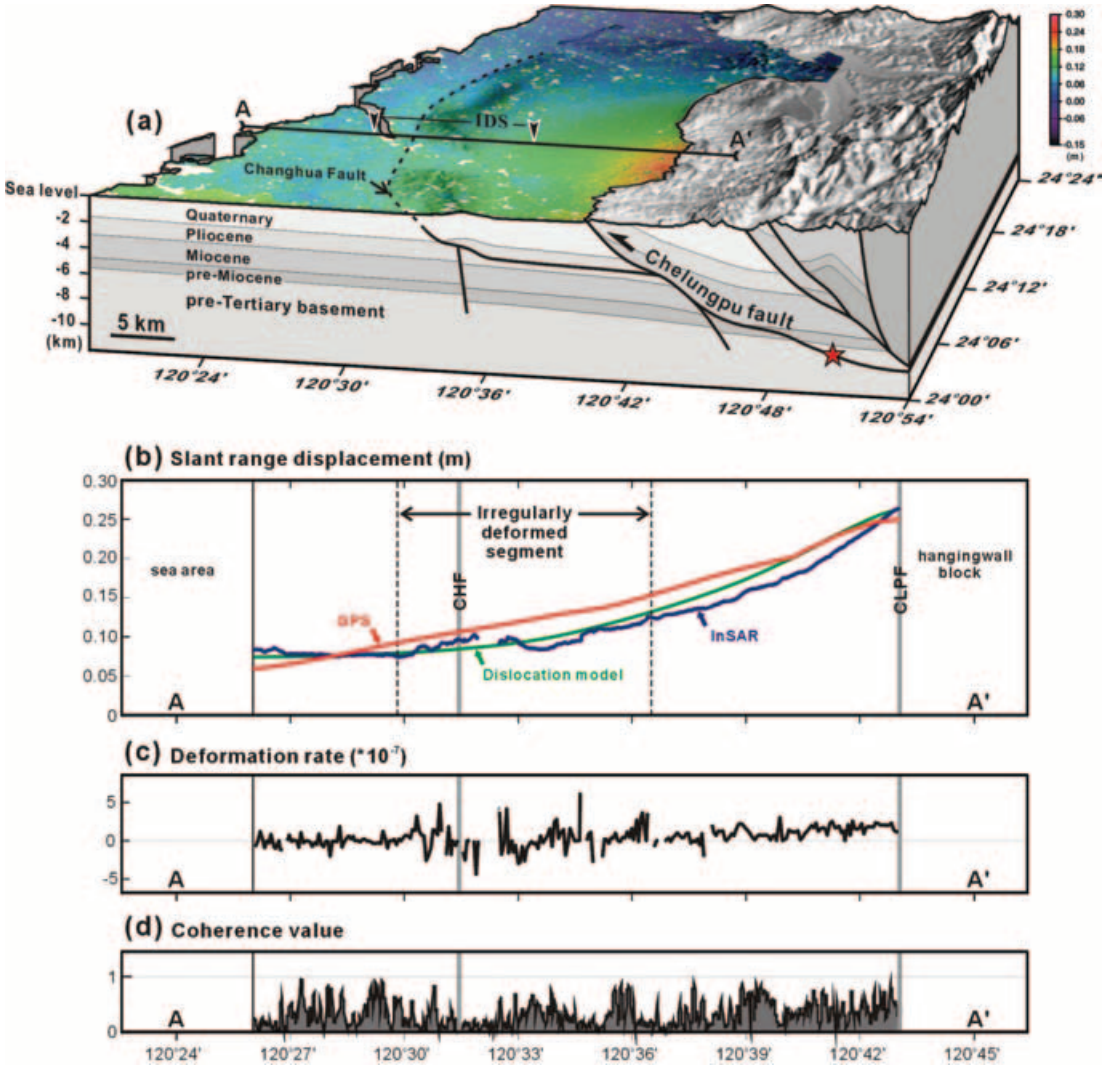

Figure 7. (a) Block diagram showing the tectonic setting of the Taichung area. The unwrapped interferogram of Fig. 8(b) is overlaid. Geological cross-section, after Mouthereau *et al.* (2001). The epicentre of the main shock is shown as a red star. (b) Slant range displacement along profile AA′ derived from different approaches. The blue line represents the measurements from the InSAR method; the red line represents the GPS measurements; and the green line shows the displacement synthesized using the elastic dislocation model. (c) The deformation gradient of profile AA′ evaluated from the InSAR observations. (d) The coherence of the images used along profile AA′.

interferometric fringes can be too complex to be distinguished when a great vertical displacement occurs in a narrow area. Moreover, the coherence of the radar image is almost lost in this case, making detection very difficult.

We can estimate the amount of surface deformation using a phase unwrapping operation. Because interferograms record only relative changes in phase, we cannot identify the fringe corresponding to no deformation in the interferogram. However, with the advantage of a dense GPS network in the area investigated, we can add a reasonable offset to all the pixels in our coseismic interferograms in the unwrapping operation. The unwrapped interferograms of pair-2 and pair-3 are shown in Figs 8(a) and (b), respectively. The maximum shortening in our unwrapped InSAR result is approximately 26 cm, which occurs around the central segment of the Chelungpu fault.

To further evaluate the effects of phase unwrapping errors in our InSAR processing, we examined the residual between the unwrapped results of pair-2 and pair-3. It shows that almost the entire footwall area exhibits a very small residual (Fig. 8c); the averaged residual is approximately 0.17 cm, the median value is approximately 0.0003 cm and the standard deviation is approximately 2.18 cm. Some parts near the northern and southern tips have a larger residual (Fig. 8c), which may be related to the unwrapping uncertainty. This test suggests to us that the unwrapping error in this study is acceptable and the deformation derived from these two interferograms is principally related to the cause of the Chichi earthquake.

The radar images of pair-4 were both acquired after the earthquake. It shows that there is one clear fringe parallel to the strike of Chelungpu fault on the footwall (Fig. 6d); this fringe represents the modest post-seismic deformation. For pair-4, because the coherence over the hangingwall area of the Chelungpu fault is better than that of pair-2 and pair-3, some coloured fringes, concentrated in certain small basins (indicated by two black cycles in Fig. 6d), can be observed. We interpret these fringes as regional subsidence or slides during the corresponding period. Further to the southwest, there are more than two cyclic fringes corresponding to land

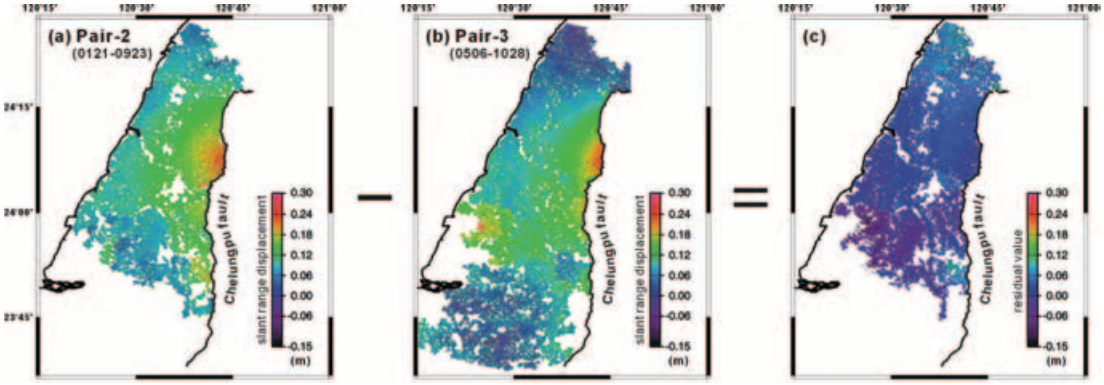

Figure 8. (a) Unwrapped interferometric result for pair-2. (b) Unwrapped interferometric result for pair-3. (c) Residual between pair-2 and pair-3. The amount of displacement is evaluated in the slant range direction. Note that same colour code in Fig. 4(a) is used in this figure.

subsidence over the lower left part of this interferogram (centre indicated by a white arrow). Considering the cyclic fringe pattern, we postulate that these land subsidences occurred as dewatering took place causing the compaction of the sediments during and after the Chichi earthquake (Watson *et al.* 2002).

Carefully comparing our interferograms, we can find some interesting cyclic fringes in the central-western part of the studied area (indicated by black arrows in Figs 6b, c and d). This cyclic fringe pattern could also be observed in the GPS simulated interferogram shown in Fig. 4(b). The coherence and continuity of the interferometric results in this area are all poor; this deformation is very difficult to estimate using unwrapping processes. We consider that, during and after the Chichi earthquake, the main shock may have produced a very large deformation in this narrow area, which could be a function of the local geological setting.

5 DISCUSSION

To better describe the detailed coseismic deformation based on our interferometric results, we sampled the slant range displacement data along a profile at latitude 24.125°N (profile AA′ in Fig. 7a and the blue line in Fig. 7b). First, we compared this profile with the GPS data (the red line in Fig. 7b) sampled from Fig. 4(a). Even though the GPS network is dense in the area investigated, many minor deformation patterns observed in the InSAR analysis cannot be seen in the GPS data (compare the red and blue lines in the Fig. 7b).

To compare our interferometric results with the elastic theory of plate deformation, we adopted the synthetic displacement determined by a computer programme, POLY3D (Chen et al. 2003). A detailed explanation of the mathematical expressions and the coding algorithm of POLY3D can be found in Thomas (1993). We directly sampled the slant range displacement data along the profile at the same latitude in this numeric model (the green line in Fig. 7b) and compared it with our interferometric result. In Fig. 7(b), we see that the modelled profile matches the interferometric profile very well; they all reflect elastic rebound of the Chelungpu fault in the footwall area (Chen et al. 2003). Such a deformation is as would be expected to affect the footwall block of a thrust fault during a large reverse-type earthquake, except for the irregularly deformed segment in the middle part of this profile.

Using the variation in slant range displacement, a segment in the middle part of this profile may be distinguished based on its anomalous deformation behaviour. We first calculate the deformation gradient along this profile (Fig. 7c). The deformation gradient is evaluated from the general slope of each 80-m window (twice the DEM grid interval). In general, the deformation gradient along this profile is less than 1×10^{-7} (Fig. 7c). However, over the irregularly deformed segment located within ∼10–20 km of the Chelungpu fault, the deformation gradient curve shows an irregular character. Note also that the coherence, signal-to-noise ratio, unwrapping error and residual fringes resulting from errors in DEM should influence the reliability of any detailed interpretation of these observations.

The coherence along this profile is shown in Fig. 7(d). A narrow section east of the Changhua fault with relative low values corresponds to an area of high signal-to-noise ratio. To avoid the effect of poor data quality, areas of low coherence and low signal-to-noise ratio have been removed from the profiles in Figs 7(b) and (c) (the blank area east of the Changhua fault). Moreover, the residual value between two coseismic interferometric results along this profile is very small (of centimetre scale; Fig. 8), so the unwrapping error should be very small. The final effect to be considered is that of topography. The orbit baseline offset of the data pair we used in this study is only 6 m (pair-3 in Fig. 5), of which the altitude of ambiguity is approximately 1570 m. Because the altitude of this irregularly deformed area is less than 300 m, the topographic effect for this area should be also very small and could therefore be neglected. Generally speaking, although some uncertainties may remain within the interferometric results, the ground displacement determined by our InSAR study is reliable in terms of providing information for characterizing the deformation of the region.

From the tectonic point of view, the irregularly deformed segment probably results from either the influence of inherited basement faults or the presence of a structural terrace that provide local opportunities for superficial deformation (Fig. 7a). The most important fault in this irregularly deformed segment is the Changhua fault, which is a blind fault and represents the deformation front of the Western Foothills of Taiwan (Deffontaines *et al.* 1997) (Figs 1 and 7a). Following the Chichi earthquake, no evident deformation has been observed by other means, whereas with its high sampling density, the InSAR technique has provided a more detailed insight, which has allowed us to determine movement associated with the earthquake.

6 CONCLUSIONS

The application of InSAR to the footwall deformation of the Chelungpu fault during the Chichi earthquake shows that, given suitable images and despite the difficulties in a subtropical area like Taiwan, differential interferometry is a useful high-resolution tool to investigate large-scale earth surface deformation. In a rather flat

study area, where the principal land covers are urban areas or mixtures of non-vegetation and vegetation such as agricultural fields, it has been shown that useful information on earthquake displacement can be obtained from C-band SAR interferograms. The poor result in the hangingwall area also illustrates the inevitable limitations of C-band InSAR in steep mountainous regions with dense vegetation. On the other hand, the very dense GPS network in the area investigated clearly enhances the value of InSAR for disaster or environmental monitoring.

In view of the westward propagation of the deformation front in Taiwan, it would appear that the footwall area of the Chelungpu fault is incubating a future large thrust, where the Pakuashan anticline and the related Changhua thrust fault are located. Our interferometric results have shown that the deformation behaviour of the Pakuashan–Changhua fold-and-thrust belt during the Chichi earthquake was different from that expected. This irregular deformation behaviour could be caused by either the activity of the Changhua fault or the compaction of Quaternary fluvial terraces.

ACKNOWLEDGMENTS

This work was supported by the National Science Council (grant no. NSC92-2119-M-008-016) and Central Geological Survey (grant no. 5226902000-03-93-04) of Taiwan. Extensive discussions with Drs J.-Y. Yen, Y.-B. Tsai and C.-C. Chen have been very helpful. Some figures were composed with the free software GMT written by Drs Paul Wessel and Walter Smith. The authors are deeply indebted to Drs E.-J. Fielding and S.-B. Yu for their helpful comments.

REFERENCES

Burgmann, R., Rosen, P.A. & Fielding, E.J., 2000. Synthetic aperture radar interferometry to measure Earth's surface topography and its deformation, *Annual Review of Earth and Planetary Science,* **28,** 169–209.

Burgmann, R. *et al.*, 2002. Deformation during the 12 Novermber 1999 Duzce, Turkey, earthquake, from GPS and InSAR data, *Bull. seism. Soc. Am.,* **92,** 161–171.

Chang, S.S.L. & Chi, W.L., 1983. Neogene nannoplakton biostratigraphy in Taiwan and the tectonic implication, *Petrol. Geol. Taiwan,* **19,** 93–147.

Chen, Y.G., Chen, W.S., Lee, J.C., Lee, Y.H., Lee, C.T., Chang, H.C. & Lo, C.H., 2001. Surface rupture of 1999 Chichi earthquake Yield insights on active tectonics of central Taiwan, *Bull. seism. Soc. Am.,* **91,** 977–985.

Chen, C.C., Chang, C.P. & Chen, K.S., 2003. Segmented faulting process of Chelungpu thrust: implication of SAR interferograms, *Terrestrial, Atmospheric and Oceanic Sciences,* **14,** 241–247.

Deffontaines, B. *et al.*, 1997. Quaternary transfer faulting in the Taiwan Foothills: evidence from a multisource approach, *Tectonophysics,* **274,** 61–82.

Delouis, B., Giardini, D., Lundgren, P. & Salichon, J., 2002. Joint inversion of InSAR, GPS, teleseismic, and strong-motion data for the spatial and temporal distribution of earthquake slip: Application to the 1999 Izmit mainshock, *Bull. seism. Soc. Am.,* **92,** 278–299.

Donnellan, A., Parker, J.W. & Peltzer, G., 2002. Combined GPS and InSAR models of postseismic deformation from the Northridge earthquake, *Pure appl. Geophys.,* **159,** 2261–2270.

Feigl, K.L. *et al.*, 2002. Estimating slip distribution for the Izmit mainshock from coseismic GPS, ERS-1, RADARSAT, and SPOT measurements, *Bull. seism. Soc. Am.,* **92,** 138–160.

Ho, C.S., 1986. A synthesis of the geologic evolution of Taiwan, *Tectonophysics,* **125,** 1–16.

Hou, C.S., Lai, T.C., Fei, L.Y. Wang, J.S. & Chen W.H., 2000. Highly accurate surveying in the study of the Chelungpu active fault-comparison of the data before and after the Chi-Chi Earthquake, *Central Geological Survey (MOEA, Taipei) Special Publication,* **12,** 191–210.

Hudnut, K. W. *et al.*, 1994. Coseismic displacement of the 1992 Landers earthquake sequence, *Bull. seism. Soc. Am.,* **84,** 625–645.

Kao, H. & Chen, W.P., 2000. The Chi-Chi earthquake sequence: active, out-of sequence thrust faulting in Taiwan, *Science,* **288,** 2346–2349.

Lee, J.C. *et al.*, 2001. A vertical exposure of the 1999 surface rupture of the Chelungpu fault at Wufeng, western Taiwan: Structural and paleoseismic implications for an active thrust fault, *Bull. seism. Soc. Am.,* **91,** 914–929.

Liew, P.M., 1988. Quaternary stratigraphy in western Taiwan: Palynological correlation, *Proc. Geol. Soc. China,* **31,** 169–180.

Ma, K.F., Lee, C.T., & Tsai, Y.B., 1999. The Chi-Chi earthquake: large surface displacement on an inland thrust fault, *EOS, Trans Am. geophys. Un.,* **80**(50), 605–611.

Ma, K.F., Song, T.R.A., Lee, S.J., & Wu, H.I., 2000. Spatial slip distribution of the September 20, 1999, Chi-Chi, Taiwan, earthquake (Mw7.6)–Inverted from Teleseismic data, *Geophys. Res. Lett.,* **27,** 3417–3420.

Massonnet, D. & Feil, K.L., 1998. Radar interferometry and its application to changes in the Earth's surface, *Rev. Geophys.,* **36,** 441–500.

Mouthereau, F., Angelier, J. & Lee J.C., 2001. Le séisme du 21 septembre 1999: influence de l'héritage structural et implication du socle au front de la chaîne de Taïwan, *C. R. Acad. Sci. Paris, Sciences de la Terre et des planetes,* **333,** 93–103.

Rubin, C., Sieh, K., Chen, Y.G., Lee, J.C., Chu, H.C., Yeats, R., Mueller, K. & Chan, Y.C., 2001. Post-earthquake response, 1999 Chi-chi earthquake: evidence for past earthquakes, *EOS, Trans Am. Geophys. Un.,* **82**(47), 565–569.

Shin, T.C., Kuo, K.W., Lee, W.H.K., Teng, T.L. & Tsai, Y.B., 2000. A preliminary report on the 1999 Chi-Chi (Taiwan) earthquake, *Seism. Res. Lett.,* **71**(1), 24–30.

Smith, W.H.F. & Wessel, P., 1990. Gridding with continuous curvature spines in tension, *Geophysics,* **55**(3), 293–305.

Sun, S.C., 1965. Geology and petroleum potentialities of the Chingshui-Yuanlin area, *Petrol. Geol. Taiwan,* **4,** 161–173.

Suppe, J., 1981. Mechanics of mountain building and metamorphism in Taiwan, *Mem. Geol. Soc. China,* **4,** 67–89.

Suppe, J., 1983. Geometry and kinematics of fault-bend folding, *Am. J. Sci,* **283,** 684–721.

Teng, T.L., Tsai, Y.B. & Lee, W.H.K., 2001. Special Issue of the Taiwan Earthquake, Preface to the 1999 Chi-Chi, Taiwan, Earthquake dedicated issue, *Bull. seism. Soc. Am.,* **91**(5), 1395 pp.

Thomas, A.L., 1993. Poly 3D: a three-dimensional, polygonal element, displacement discontinuity boundary element computer program with applications to fractures, faults, and cavities in the Earth's crust, *MSc thesis,* Stanford University, Stanford, CA, USA.

Tsai, Y.B., 1986. Seismotectonics of Taiwan, *Tectonophysics,* **125,** 17–37.

Watson, K.M., Bock, Y. & Sandwell, D.T., 2002. Satellite interferometric observations of displacements associated with seasonal groundwater in the Los Angeles Basin, *J. geophys. Res.,* **107**(B4), ETG8-1—ETG8-12.

Wright, T.J., Rarsons, B.E., Jackson, J.A., Haynes, M., Fielding, E.J., England, P.C. & Clarke, P.J., 1999. Source parameters of the 1 October 1995 Dinar(Turkey) earthquake from SAR interferometry and seismic bodywave modeling, *Earth planet. Sci. Lett.,* **172,** 23–37.

Yu, S.B., Chen, H.Y. & Kuo, L.C., 1997. Velocity field of GPS stations in the Taiwan area, *Tectonophysics,* **274,** 41–59.

Yu, S.B. *et al.*, 2001. Preseismic deformation and coseismic displacements associated with the 1999 Chi-Chi, Taiwan, Earthquake, *Bull. seism. Soc. Am.,* **91,** 995–1012.

Zebker, H.A., Rosen, P.A., Goldstein, R.M., Gabriel, A. & Werner, C.L., 1994. On the derivation of coseismic displacement fields using differential radar interferometry: The Landers earthquake, *J. geophys. Res.,* **99,** 19 617–19 634.